

The multiscale formulation of large eddy simulation: Decay of homogeneous isotropic turbulence

Thomas J. R. Hughes,^{a)} Luca Mazzei, and Assad A. Oberai
Division of Mechanics and Computation, W. F. Durand Building, Stanford University, Stanford, California 94305-4040

Alan A. Wray
NASA Ames Research Center, Moffett Field, California 94035

(Received 10 May 2000; accepted 23 October 2000)

The variational multiscale method is applied to the large eddy simulation (LES) of homogeneous, isotropic flows and compared with the classical Smagorinsky model, the dynamic Smagorinsky model, and direct numerical simulation (DNS) data. Overall, the multiscale method is in better agreement with the DNS data than both the Smagorinsky model and the dynamic Smagorinsky model. The results are somewhat remarkable when one realizes that the multiscale method is almost identical to the Smagorinsky model (the least accurate model!) except for removal of the eddy viscosity from a very small percentage of the lowest modes. © 2001 American Institute of Physics. [DOI: 10.1063/1.1332391]

I. INTRODUCTION

Large eddy simulation (LES) has proven to be a valuable technique for the calculation of turbulent flows. The philosophy of LES consists of resolving large-scale flow features and modeling subgrid-scale stresses, which represent the effect of missing, unresolved scales on resolved scales within the filtered Navier–Stokes equations. The Smagorinsky eddy viscosity model¹ has played a dominant role in LES over the years. The classical Smagorinsky model entails definition of a constant, a length scale and a time scale. *A priori* analyses to determine the constant and length scale have been performed by Lilly.^{2–4} Lilly employs the Kolmogorov energy spectrum and assumptions relating mesh scales to the cut-off wave number of the discretization. Experience has revealed that the constant determined by this process is not suitable for all flows. In addition, many other shortcomings of the Smagorinsky model have been identified, such as incorrect asymptotics in wall-bounded flows, inability to accommodate backscatter, excessive dissipation in the presence of large coherent structures, incorrect growth rate of perturbations in transition, etc. (see, e.g., Germano *et al.*⁵ and Piomelli⁶). These have prompted numerous efforts to improve upon the Smagorinsky model. A major advance took place with the development of the dynamic Smagorinsky model^{5,7,8} in which the Smagorinsky constant is replaced with a function of space and time which is self-adaptively determined along with the flow solution. The dynamic Smagorinsky model has led to improved results in almost all cases (see Piomelli⁶ for a recent review and assessment of the state-of-the-art). Nevertheless, many efforts have been

devoted to further improvement. For example, we may mention “mixed-models”⁹ and “scale-similar models.”¹⁰

A new philosophy of LES was espoused in Hughes *et al.*,¹¹ where it was argued that many shortcomings of Smagorinsky-based approaches were associated with their inability to successfully differentiate between large and small scales. To this end, a multiscale method was adopted to perform scale-separation *ab initio*. The idea of using multiscale approaches in turbulence is not new. Temam and his colleagues have been pursuing this strategy for a number of years (see Dubois, Jauberteau, and Temam^{12–14}). Our work began in Hughes¹⁵ and Hughes and Stewart¹⁶ where the initial focus was more on explaining and refining certain “good” numerical methods than on turbulence modeling. The inextricable relationship between modeling and good numerical methods was emphasized in Hughes *et al.*¹⁷ The main tenets of our approach are summarized as follows:

- (i) Variational projection is used to differentiate scales.
- (ii) *A priori* scale separation is preferred to attempts at *a posteriori* scale separation. This enables surgical modeling of unresolved, high wave-number phenomena rather than all wave numbers, as in contemporary LES.
- (iii) Modeling is confined to the small-scale equation in preference to modeling within the large-scale equation.

It can be argued that, even with relatively crude modeling, such as using a constant-coefficient Smagorinsky model in the small-scale equation, many of the shortcomings of the traditional LES models are obviated. These points were made in Hughes *et al.*¹¹ but no numerical results were presented supporting them. In this work we take a first step in providing numerical verification of our ideas. Here, we examine homogeneous, isotropic flows using a spectral

^{a)}Author to whom correspondence should be addressed. Telephone: 650-723-2040; Fax: 650-723-1778; electronic mail: hughes@am-sun2.stanford.edu

method. The variational multiscale method has a transparent interpretation in the context of spectral methods.

We note in passing that our original presentation of the variational multiscale methods for LES (Ref. 11) was concerned with physical, rather than spectral, space. Therein we described variational/finite element formulations using hierarchical bases and ‘‘bubbles,’’ which are useful techniques for developing multiscale procedures. Jansen¹⁸ has implemented the methods with success in a stabilized finite element code employing hierarchical bases. We believe similar ideas can also be developed for finite difference and finite volume codes by exploiting technology used in multigrid solvers, in particular, agglomeration operators which can be used to extract large-scale subspaces. This approach is being pursued by Farhat.¹⁹ It could also be used in finite element codes.

The remainder of the paper is summarized as follows: in Sec. II we describe the spectral variational multiscale method. In Sec. III, we present numerical results for a homogeneous, isotropic Euler flow, and for the decay of homogeneous, isotropic turbulence with initial Taylor microscale Reynolds number of about 90. The methods compared are the standard Smagorinsky model, the dynamic Smagorinsky model, and two variants of the multiscale method. All results are benchmarked against direct numerical simulation (DNS) data. The multiscale results are in better agreement with the DNS data than both the Smagorinsky and dynamic Smagorinsky models. Furthermore, we argue that the multiscale results are not optimized in any way. Conclusions are presented in Sec. IV.

II. THEORY

The variational multiscale method for LES was introduced by Hughes *et al.*¹¹ Here we will provide a brief description specialized for the case of a spectral method. For a comprehensive presentation of spectral methods, see Canuto *et al.*²⁰

We consider the incompressible, isothermal, Navier–Stokes equations on the spatial domain $\Omega = [0, 2\pi]^3 \subset \mathbb{R}^3$. We assume periodic boundary conditions in all three spatial directions. In this case we have

$$\frac{\partial \mathbf{u}}{\partial t} + \nabla \cdot (\mathbf{u} \otimes \mathbf{u}) + \nabla p = \nu \Delta \mathbf{u} \quad \text{in } \mathbf{Q}, \tag{1}$$

$$\nabla \cdot \mathbf{u} = 0 \quad \text{in } \mathbf{Q}, \tag{2}$$

$$\mathbf{u}(\mathbf{x}, 0) = \mathbf{u}_0(\mathbf{x}) \quad \text{on } \Omega, \tag{3}$$

where \mathbf{u} is the velocity vector, p is the pressure, ν is the kinematic viscosity, $\mathbf{Q} = \Omega \times]0, T[$, T defines the time interval of interest, and \mathbf{u}_0 is the given initial velocity, assumed divergence free. Let the boundary of Ω be denoted by $\partial\Omega$. It is comprised of six faces, $\Gamma_j(0)$, $\Gamma_j(2\pi)$, $j = 1, 2, 3$, where

$$\Gamma_j(c) = \{\mathbf{x} \in \partial\Omega | x_j = c\}. \tag{4}$$

The periodic boundary conditions may be expressed as

$$\begin{aligned} \mathbf{u}(\mathbf{y}, t) &= \mathbf{u}(\mathbf{x}, t), & \mathbf{x} \in \Gamma_j(0), \\ \mathbf{y} &= \mathbf{x} + 2\pi \mathbf{e}_j \in \Gamma_j(2\pi), & t \in]0, T[, \end{aligned} \tag{5}$$

where \mathbf{e}_j is the unit Cartesian basis vector in the x_j direction.

The Fourier series representation of the solution is

$$\mathbf{u}(\mathbf{x}, t) = \sum_{\mathbf{k}} \hat{\mathbf{u}}_{\mathbf{k}}(t) e^{i\mathbf{k} \cdot \mathbf{x}}, \tag{6}$$

$$p(\mathbf{x}, t) = \sum_{\mathbf{k}} \hat{p}_{\mathbf{k}}(t) e^{i\mathbf{k} \cdot \mathbf{x}}, \tag{7}$$

where $\mathbf{k} = (k_1, k_2, k_3)$ is the wave-number vector and $\hat{\mathbf{u}}_{\mathbf{k}}$ and $\hat{p}_{\mathbf{k}}$ are the Fourier coefficients of \mathbf{u} and p , respectively. The Fourier versions of (1) and (2) are, respectively,

$$\left(\frac{d}{dt} + \nu |\mathbf{k}|^2 \right) \hat{\mathbf{u}}_{\mathbf{k}} = -i\mathbf{k} \hat{p}_{\mathbf{k}} - i\mathbf{k} \cdot \widehat{(\mathbf{u} \otimes \mathbf{u})}_{\mathbf{k}}, \tag{8}$$

$$i\mathbf{k} \cdot \hat{\mathbf{u}}_{\mathbf{k}} = 0. \tag{9}$$

The Fourier–Galerkin approximation truncates the sums, (6) and (7), such that $-n/2 \leq k_j \leq +n/2 - 1$, $j = 1, 2, 3$. This corresponds to a direct numerical simulation (DNS) with a grid of n^3 cells. Note that, modes for which $k_j = -n/2$, $j = 1, 2, 3$, are omitted for reasons concerning commonly used FFT’s (see discussion on p. 78 of Canuto *et al.*²⁰). In practice, one does not use the pressure. The velocity is simply projected on its divergence-free part employing (9).

A. Smagorinsky model

As a point of reference for describing the multiscale models, we will first present the Smagorinsky model. In this case the subgrid-scale stress is modeled by

$$\mathbf{T} = 2\nu_T \nabla^s \mathbf{u}, \tag{10}$$

where

$$\nu_T = (C_S \Delta)^2 |\nabla^s \mathbf{u}| \tag{11}$$

in which C_S is the so-called Smagorinsky constant, Δ is a length scale, $\nabla^s \mathbf{u}$ denotes the symmetric gradient, viz.,

$$\nabla^s \mathbf{u} = \frac{1}{2} (\nabla \mathbf{u} + (\nabla \mathbf{u})^T) \tag{12}$$

and

$$|\nabla^s \mathbf{u}| = (2\nabla^s \mathbf{u} \cdot \nabla^s \mathbf{u})^{1/2}. \tag{13}$$

The length scale Δ is taken to be the mesh size. The modeled counterpart of (8) is

$$\left(\frac{d}{dt} + \nu |\mathbf{k}|^2 \right) \hat{\mathbf{u}}_{\mathbf{k}} = -i\mathbf{k} \hat{p}_{\mathbf{k}} - i\mathbf{k} \cdot [\widehat{(\mathbf{u} \otimes \mathbf{u})}_{\mathbf{k}} - \hat{\mathbf{T}}_{\mathbf{k}}]. \tag{14}$$

B. Multiscale formulation

In the multiscale formulation we decompose the solution into large-scale and small-scale components, viz.,

$$\mathbf{u} = \bar{\mathbf{u}} + \mathbf{u}', \tag{15}$$

$$p = \bar{p} + p', \tag{16}$$

where

$$\bar{\mathbf{u}}(\mathbf{x}, t) = \sum_{|\mathbf{k}| < n/2} \hat{\mathbf{u}}_{\mathbf{k}}(t) e^{i\mathbf{k} \cdot \mathbf{x}}, \tag{17}$$

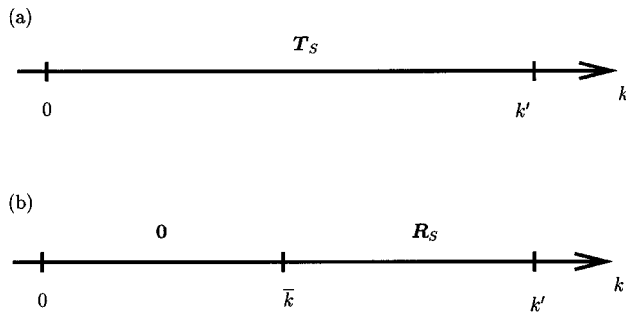


FIG. 1. Comparison of classical LES (a) with multiscale LES (b).

$$\bar{p}(\mathbf{x}, t) = \sum_{|\mathbf{k}| < \bar{n}/2} \hat{p}_{\mathbf{k}}(t) e^{i\mathbf{k} \cdot \mathbf{x}}, \tag{18}$$

$$\mathbf{u}'(\mathbf{x}, t) = \sum_{|\mathbf{k}| \geq \bar{n}/2} \hat{\mathbf{u}}_{\mathbf{k}}(t) e^{i\mathbf{k} \cdot \mathbf{x}}, \tag{19}$$

$$p'(\mathbf{x}, t) = \sum_{|\mathbf{k}| \geq \bar{n}/2} \hat{p}_{\mathbf{k}}(t) e^{i\mathbf{k} \cdot \mathbf{x}}, \tag{20}$$

$$|\mathbf{k}| = (k_1^2 + k_2^2 + k_3^2)^{1/2}, \tag{21}$$

and $\bar{n} < n'$. The sums in (19) and (20) are truncated by $-n'/2 \leq k_j \leq n'/2 - 1, j = 1, 2, 3$, where n' defines the LES grid.

Modeling is confined to the small scales, i.e., let

$$\mathbf{R} = 2\nu_T' \nabla^s \mathbf{u}', \tag{22}$$

where there are two choices under consideration for ν_T' ,

$$\nu_T' = (C_S' \Delta')^2 |\nabla^s \mathbf{u}'| \tag{23}$$

and

$$\nu_T' = (C_S' \Delta')^2 |\nabla^s \bar{\mathbf{u}}|. \tag{24}$$

We refer to (23) as ‘‘small–small’’ and to (24) as ‘‘large–small.’’ The length scale Δ' is taken to be the mesh size. The equations in Fourier space are

$$\left(\frac{d}{dt} + \nu |\mathbf{k}|^2 \right) \hat{\mathbf{u}}_{\mathbf{k}} = -i\mathbf{k} \hat{p}_{\mathbf{k}} - i\mathbf{k} \cdot (\widehat{\mathbf{u} \otimes \mathbf{u}})_{\mathbf{k}} \quad |\mathbf{k}| < \bar{n}/2, \tag{25}$$

$$\left(\frac{d}{dt} + \nu |\mathbf{k}|^2 \right) \hat{\mathbf{u}}_{\mathbf{k}} = -i\mathbf{k} \hat{p}_{\mathbf{k}} - i\mathbf{k} \cdot [(\widehat{\mathbf{u} \otimes \mathbf{u}})_{\mathbf{k}} - \hat{\mathbf{R}}_{\mathbf{k}}] \tag{26}$$

$$\begin{aligned} \bar{n}/2 \leq |\mathbf{k}|, \\ -n'/2 \leq k_j \leq n'/2 - 1, j = 1, 2, 3. \end{aligned}$$

Equations (25) and (26) are coupled through the convective term, and in the case of large–small through the model term. A schematic comparison of the multiscale version of LES with the traditional LES formulation is presented in Fig. 1.

III. NUMERICAL RESULTS

A. Preliminaries

The code employed for the simulations was written by Wray. Spatial differentiation is by the Fourier spectral

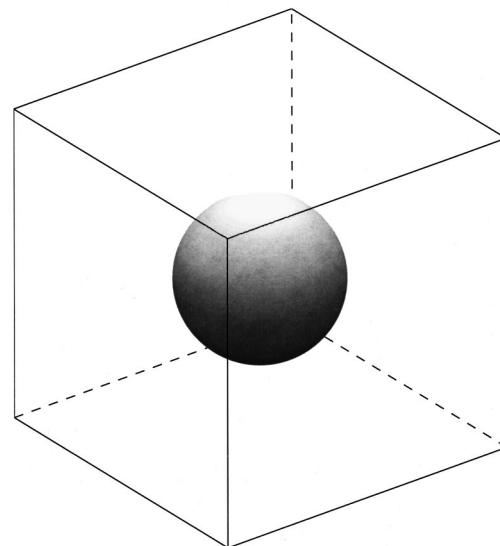


FIG. 2. Cube in wave-vector space representing the space \mathcal{F} , and sphere representing the space $\tilde{\mathcal{F}}$. The space $\mathcal{F}' = \mathcal{F} \setminus \tilde{\mathcal{F}}$.

method (see Orszag and Patterson²¹). Time advancement is by a four-step, third-order Runge–Kutta method. All terms are dealiased with the 3/2 rule (see Canuto *et al.*²⁰); within round-off this eliminates aliasing errors for convective terms, but the LES models involve higher-order functions (e.g., square-root) and so are not dealiased by the 3/2 rule. Molecular viscous effects are accounted for by an exponential integrating factor. The methods compared are:

- (1) DNS;
- (2) Smagorinsky ($C_S = 0.1$);
- (3) dynamic Smagorinsky with sharp cut-off (Germano *et al.*,⁵ Ghosal *et al.*,^{7,8} Lilly²²);
- (4) multiscale ($C_S' = 0.1$), small–small, large–small.

For the same resolution, the computational cost of the various LES methods is not substantially different. The least expensive methods are Smagorinsky and small–small, which are comparable. Large–small is about 25% more expensive and the dynamic model is over two times more expensive.

For the multiscale models with resolution $n'^3, \bar{n} = n'/2$. This can be schematically represented in wave-

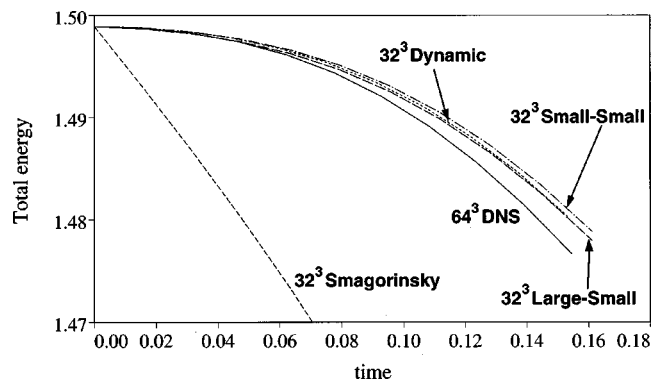


FIG. 3. Inviscid case: Total energy, $E(k \leq 15)$ vs time.

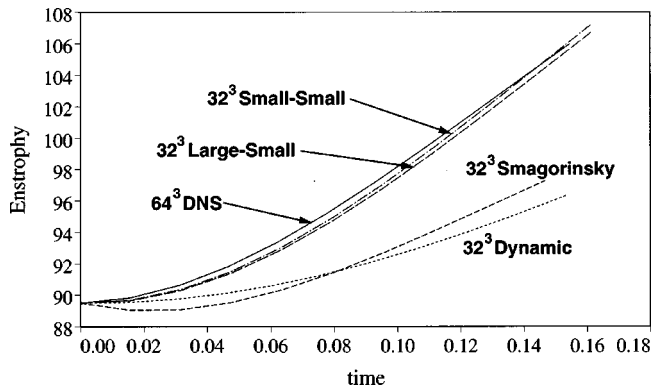


FIG. 4. Inviscid case: Enstrophy, $D(k \leq 15)$ vs time.

vector space as follows: The space \mathcal{V} is represented by a cube, centered at the origin and aligned with the coordinate axes, with edge length $n' - 1$. The large-scale space, \mathcal{V}' , is depicted roughly by a sphere with diameter $n'/2$, centered at the origin (see Fig. 2). The small-scale space, $\mathcal{V}'' = \mathcal{V} \setminus \mathcal{V}'$, is the cube with the sphere removed. The fraction of functions associated with the large-scale space is the ratio of the volume of the sphere to the volume of the cube, viz., $(\pi/6)(n'/2)^3/(n'-1)^3$. We performed multiscale calculations with $n' = 32$ and $n' = 64$. For these cases, the percentages of large-scale functions are only 7.2% and 6.9%, respectively. Nevertheless, the differences engendered by omitting the eddy viscosity in the large-scale equation will be seen to be significant.

B. Inviscid case

The calculations depict the early time dynamics of the incompressible Euler equations. Long time results are not useful because of unphysical pile-up of energy in small scales.

The energy spectrum of the initial data is proportional to $k^4 \exp(-4k/k_p)$, where $k_p = 4.0$ is the location of the peak value, and the phases are random.

The reference DNS is performed with 64^3 resolution. The LES calculations are all performed with 32^3 resolution.

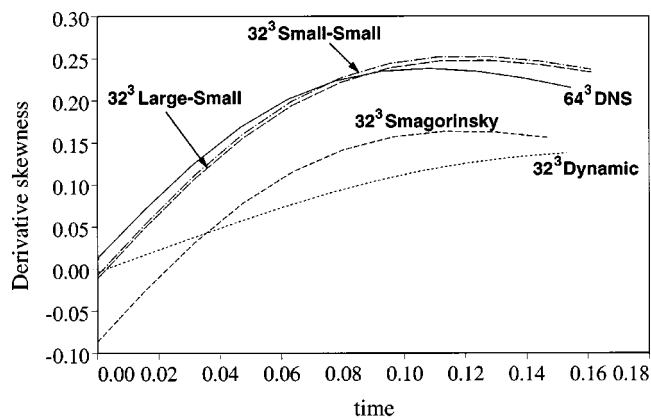


FIG. 5. Inviscid case: Derivative skewness, $S(k \leq 15)$ vs time.

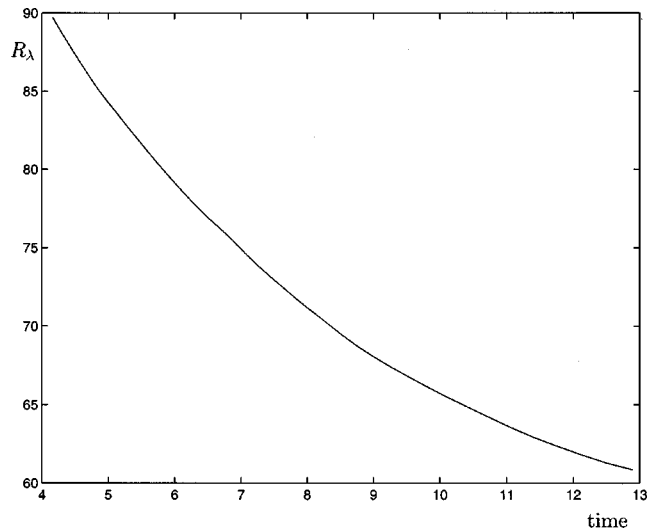


FIG. 6. Viscous case: Taylor microscale Reynolds number, R_λ vs time.

The decay of total resolved energy is presented in Fig. 3. The dynamic Smagorinsky and multiscale models track the DNS data well, exhibiting decay $\sim t^2$, whereas the Smagorinsky results are clearly much too dissipative, exhibiting decay $\sim t$.

Enstrophy results are presented in Fig. 4. In contrast with energy, which is dominated by low wave-number components, enstrophy accentuates the higher wave-number behavior. The multiscale models agree very well with the DNS data while the dynamic Smagorinsky and Smagorinsky models deviate substantially.

The slopes of the Smagorinsky energy and enstrophy results at $t=0.0$ are negative, while all other models and DNS have the correct zero slopes. The zero slopes at $t = 0.0$ for the dynamic Smagorinsky model can be explained by the fact that the initial data has random phases which produce zero C_S . In the multiscale methods, the eddy viscosity is zero for $k < 8$. The peaks of the energy and enstrophy spectra are at $k = 4$ and $k = 6$, respectively, and the spectra decrease rapidly for larger values of k . Thus initially there is very little energy and enstrophy for modes in which the eddy viscosity is nonzero.

Skewness results are presented in Fig. 5. The production of the rate of dissipation of turbulent kinetic energy or,

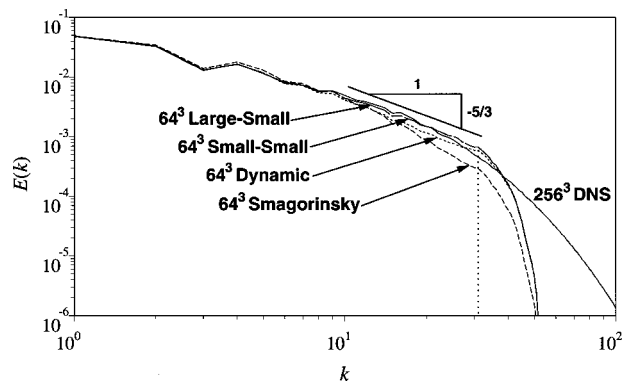


FIG. 7. Viscous case: Energy, $E(k)$, at $t = 6.47$.

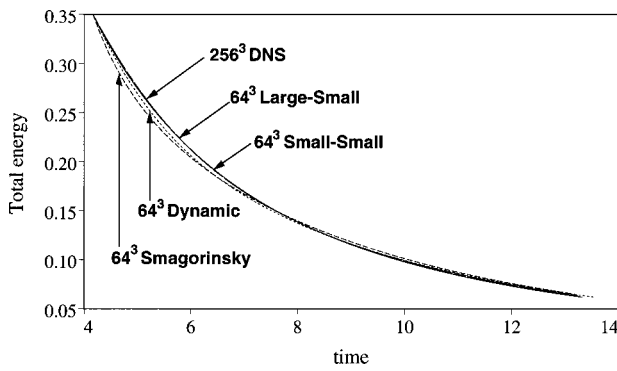


FIG. 8. Viscous case: Total energy, $E(k \leq 31)$ vs. time.

equivalently, the production of enstrophy, is directly related to skewness.²³ Note, the effect of the model is incorporated in our definition of skewness, which is computed in the usual spectral way in terms of the energy transfer function, $T(k)$, which includes the effect of the model (see Monin and Yaglom,²⁴ p. 240),

$$S = - \frac{\langle (\partial u_1 / \partial x_1)^3 \rangle}{\langle (\partial u_1 / \partial x_1)^2 \rangle^{3/2}} = \frac{3\sqrt{30}}{14} \frac{\int_0^\infty k^2 T(k) dk}{[\int_0^\infty k^2 E(k) dk]^{3/2}}, \quad (27)$$

$$S(k \leq \bar{k}) = \frac{3\sqrt{30}}{14} \frac{\int_0^{\bar{k}} k^2 T(k) dk}{[\int_0^{\bar{k}} k^2 E(k) dk]^{3/2}}. \quad (28)$$

In (27), $\langle \cdot \rangle$ denotes spatial integration over $\Omega = [0, 2\pi]^3$. The Smagorinsky and dynamic Smagorinsky models exhibit considerable deviation from the DNS data, whereas the multiscale models are again in good agreement.

Although differences between the large-small and small-small multiscale results for the inviscid case are discernible, they are very small.

C. Viscous case

The viscous initial conditions are determined from a truncation of a developed 256^3 turbulence field at time 4.16. The time zero initial condition is of the same form as the inviscid case with $k_p = 1.0$.

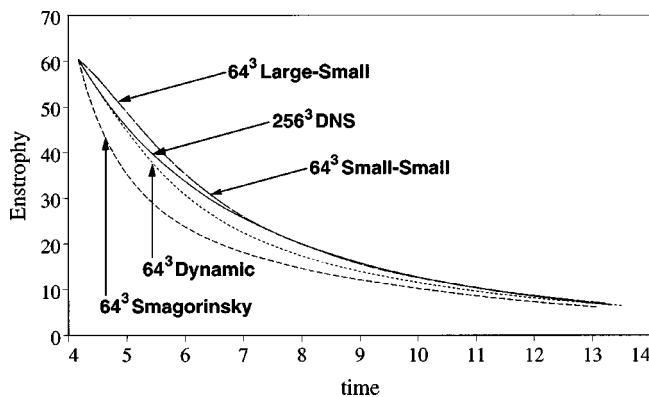


FIG. 9. Viscous case: Enstrophy, $D(k \leq 31)$ vs. time.

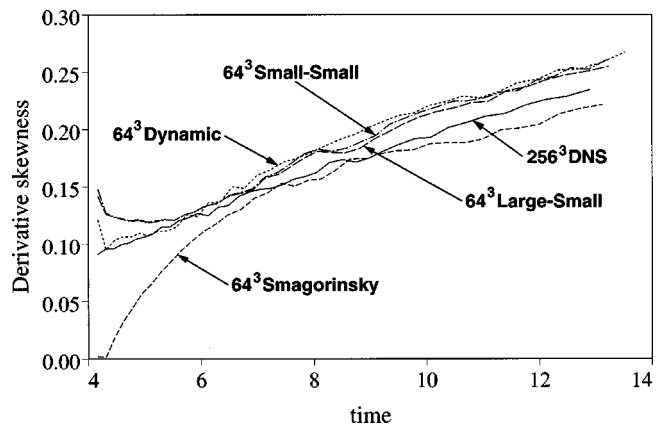


FIG. 10. Viscous case: Derivative skewness, $S(k \leq 31)$ vs. time.

The reference DNS is performed at 256^3 and the LES calculations are performed at 64^3 . Figure 6 shows the Taylor microscale Reynolds number, R_λ , over the course of the simulation.

In Fig. 7, energy spectra are presented at $t = 6.47$. It is apparent that the Smagorinsky results are the most dissipative, significantly underestimating the DNS data for $k \geq 10$. The dynamic Smagorinsky model is better, but also underestimates the DNS data for $k \geq 10$, before crossing over at about $k = 30$. The results of both multiscale models are virtually identical and are in good agreement with the DNS data up to $k = 20$ and then slightly overestimate them between $k = 20$ and $k = 30$. Beyond $k = 30$, we exceed the resolution limit and the LES results are not meaningful.

The decay of total resolved energy is presented in Fig. 8. Both multiscale models coincide with the DNS data throughout the entire analysis. The Smagorinsky model is the most dissipative early on but slightly crosses over the DNS data beyond $t = 8.0$. The dynamic Smagorinsky model is also too dissipative early on but matches the DNS data very well beyond $t = 8.0$.

The decay of resolved enstrophy is presented in Fig. 9. The Smagorinsky model results differ significantly from the DNS data and are again the least accurate of all the models. The dynamic Smagorinsky model results exhibit good agreement early on, the initial slope coinciding with that of the DNS data, but then deviate substantially thereafter. The mul-

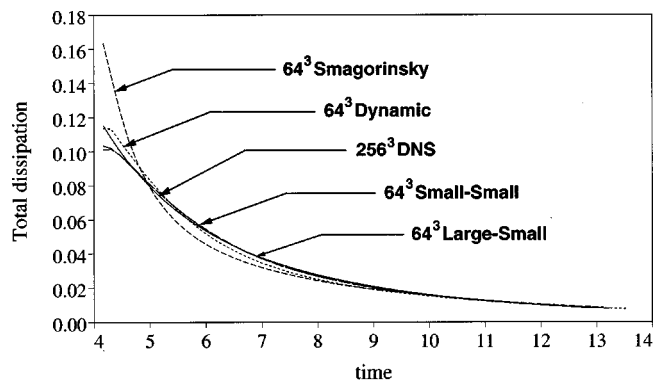


FIG. 11. Viscous case: Total dissipation vs. time.

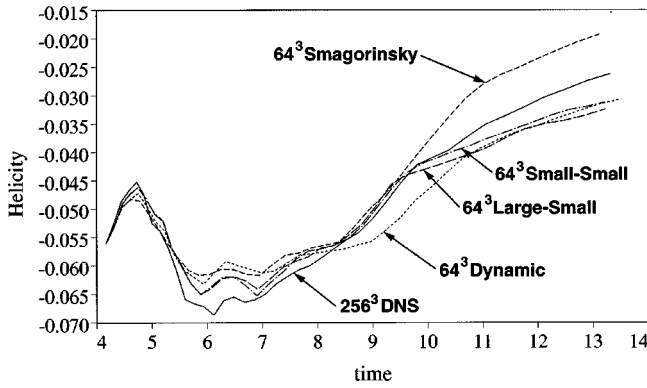


FIG. 12. Viscous case: Helicity, $H(k \leq 31)$ vs time.

tiscale method results are not as accurate as those for the dynamic Smagorinsky model up to $t \approx 5.6$, but the trend reverses thereafter, and beyond $t = 7.0$ the multiscale results essentially coincide with the DNS data.

Resolved derivative skewness results are presented in Fig. 10. After an initial transient, all the models are in fair agreement with the DNS data with no particular model showing clear superiority.

Total dissipation is presented in Fig. 11. The Smagorinsky model is again the least accurate. Initially it exhibits too much dissipation but crosses over the DNS data at $t \approx 5.0$. The dynamic Smagorinsky model follows a similar trend, crossing over at about $t = 6.0$, but it is considerably more accurate than the Smagorinsky model. The multiscale models are clearly the most accurate, showing excellent agreement with the DNS data for $t \geq 4.6$.

Resolved helicity results are presented in Fig. 12. The models only achieve fair accuracy in approximating the DNS helicity data. The multiscale models are the most accurate overall, the dynamic Smagorinsky model is intermediate, and the Smagorinsky model is the least accurate. The small–small multiscale model is slightly better than the large–small model.

As in the inviscid case, only very small differences between the two multiscale versions can be discerned and these are not significant enough to conclude one version is superior to the other.

Overall, we conclude that the multiscale models are the most accurate models. The dynamic Smagorinsky model is intermediate and the Smagorinsky model is the least accurate.

D. The small-scale Smagorinsky constant

We wish to emphasize that no tuning was performed to obtain an optimal small-scale Smagorinsky constant, C'_S , for the multiscale models. The value $C'_S = 0.1$ was selected to be the same value used for the Smagorinsky model. There is no *a priori* reason why this is a good choice. It is therefore interesting to examine this issue. To this end we shall perform an analysis like that of Lilly²⁻⁴ for the case at hand. In particular, we equate turbulent kinetic energy dissipation, ϵ , with model dissipation. We assume the cut-off wave number is k' , and the length scale $\Delta = \Delta'$, i.e., we assume all the

models employ the same resolution, as was the case in our calculations. As a prelude to the analysis of the multiscale models, let us review the Lilly calculation for the Smagorinsky model, viz.,

$$\epsilon = 2(C_S \Delta')^2 |\nabla^s \mathbf{u}| (\nabla^s \mathbf{u} \cdot \nabla^s \mathbf{u}) = (C_S \Delta')^2 |\nabla^s \mathbf{u}|^3, \quad (29)$$

where $|\nabla^s \mathbf{u}| = (2 \nabla^s \mathbf{u} \cdot \nabla^s \mathbf{u})^{1/2}$ is evaluated from

$$\frac{1}{2} |\nabla^s \mathbf{u}|^2 = \int_0^{k'} k^2 E(k) dk \quad (30)$$

with

$$E(k) = \alpha \epsilon^{2/3} k^{-5/3} \quad (31)$$

in which α is the Kolmogorov constant, $E(k)$ is the spectral amplitude of kinetic energy, defined as the integral over surfaces of spheres in wave-number space parametrized by the radius k , and (31) expresses the assumption that the cut-off wave number, k' , is in the inertial subrange. This leads to

$$C_S \Delta' = \left(\frac{2}{3\alpha}\right)^{3/4} k'^{-1}. \quad (32)$$

Now we perform similar calculations for the multiscale models. We begin with the case of small–small,

$$\epsilon = 2(C'_S \Delta')^2 |\nabla^s \mathbf{u}'| (\nabla^s \mathbf{u}' \cdot \nabla^s \mathbf{u}') = (C'_S \Delta')^2 |\nabla^s \mathbf{u}'|^3, \quad (33)$$

where

$$\frac{1}{2} |\nabla^s \mathbf{u}'|^2 = \int_{\bar{k}}^{k'} k^2 E(k) dk. \quad (34)$$

This leads to

$$C'_S \Delta' = \left(\frac{2}{3\alpha}\right)^{3/4} \bar{k}^{-1} [(k'/\bar{k})^{4/3} - 1]^{-3/4}. \quad (35)$$

For the case of large–small, we have

$$\epsilon = 2(C'_S \Delta')^2 |\nabla^s \bar{\mathbf{u}}| (\nabla^s \bar{\mathbf{u}} \cdot \nabla^s \bar{\mathbf{u}}) = (C'_S \Delta')^2 |\nabla^s \bar{\mathbf{u}}| |\nabla^s \bar{\mathbf{u}}|^2 \quad (36)$$

and thus

$$C'_S \Delta' = \left(\frac{2}{3\alpha}\right)^{3/4} \bar{k}^{-1} [(k'/\bar{k})^{4/3} - 1]^{-1/2}. \quad (37)$$

The ratio C'_S/C_S is plotted vs k'/\bar{k} in Fig. 13 for the two multiscale models. One use for these results is that if one has determined a “good” value of the Smagorinsky constant, C_S , then good values of C'_S follow. Viewing C_S as given, and k' fixed, C'_S becomes a function of the choice of \bar{k} . Note the obvious fact that $C'_S/C_S > 1$, which can also be gleaned from Fig. 13. As $\bar{k} \rightarrow 0$, $C'_S/C_S \rightarrow 1$ for small–small, whereas $C'_S/C_S = O((k'/\bar{k})^{1/3})$ for large–small.

In order to assess the value of C'_S chosen for the simulations, we need to determine k'/\bar{k} . In the viscous case $\bar{k} = 15$. Keeping in mind that k' is the radius of a sphere in the Lilly analysis, we shall calculate k' to be the radius of the sphere having volume 63^3 (see Fig. 14). Thus, $\frac{4}{3}\pi(k')^3$

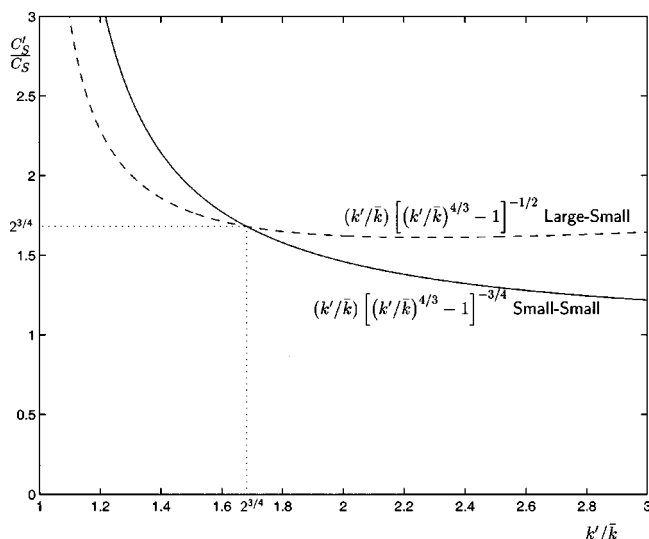


FIG. 13. C'_S/C_S vs k'/\bar{k} for the multiscale models.

$=63^3$ and so $k'/\bar{k}=2.60$. For this value, Fig. 13 suggests that the desired ratios of the Smagorinsky constants are given by

$$C'_S/C_S = \begin{cases} 1.28 & \text{small-small} \\ 1.62 & \text{large-small.} \end{cases} \quad (38)$$

We also remark that experience with the code employed suggested that $C_S=0.1$ was a “good” value for the Smagorinsky model, although for the particular case studied it appears to yield results that are somewhat too dissipative.

In order to see if the trend suggested by these results is correct we performed a sweep of C'_S for the small-small case. Figure 15 depicts the total dissipation for $C'_S=0$ (no model), 0.05, 0.1 (the value used for the simulations previously presented), and 0.2. We note that the result for $C'_S=0.1$ was presented already in Fig. 11. However, in Fig. 15 the scale of the plot is such that small deviations are more

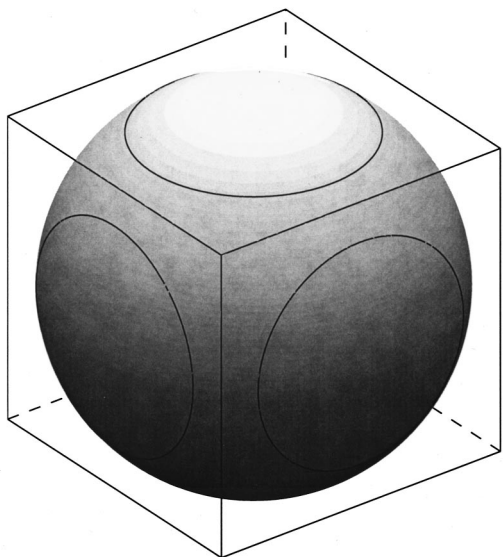


FIG. 14. Cube and volume-equivalent sphere in wave-vector space.

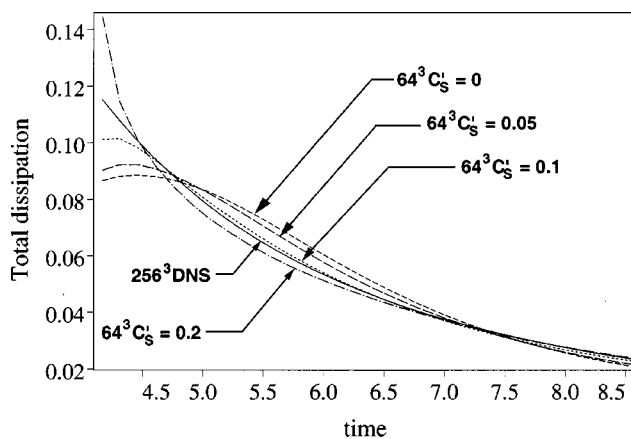


FIG. 15. Viscous case: Total dissipation for different values of C'_S . The multiscale model used was small-small.

clearly visible than in Fig. 11. It can be seen that the best value for C'_S would lie between 0.1 and 0.2, but closer to 0.1. We conclude that the value 0.1 was not a bad choice, but also not the best choice. Consequently, the results obtained in the simulations may be viewed as representative rather than optimized in favor of the multiscale methods.

IV. CONCLUSIONS

We have tested the variational multiscale method on homogeneous, isotropic flows. Comparisons have been made with the standard Smagorinsky model, the dynamic Smagorinsky model, and DNS data. Overall, the multiscale methods are in better agreement with DNS data than both the Smagorinsky and dynamic Smagorinsky models, despite the fact that we used unoptimized, constant-coefficient eddy viscosities in the multiscale methods.

We attribute the good results obtained to basic features of the variational multiscale method, namely, modeling is confined to the equations governing small scales, where there seems to be less sensitivity to the particular form of the modeling, as evidenced by the quality of the results obtained with a Smagorinsky-type model. Nevertheless, it is still somewhat remarkable that the multiscale results are as good as they are when one realizes that the main difference between the multiscale method used and the standard Smagorinsky model is simply removal of the eddy viscosity from a small percentage of the lowest resolved modes.

ACKNOWLEDGMENTS

We wish to thank P. Moin for facilitating this study. This research was supported by NASA Ames Research Center Cooperative Agreement No. NCC 2-5363 and ONR Grant No. 00014-99-1-0122. This support is gratefully acknowledged.

¹J. Smagorinsky, “General circulation experiments with the primitive equations. I. The basic experiment,” *Mon. Weather Rev.* **91**, 99 (1963).
²D. K. Lilly, “On the application of the eddy viscosity concept in the inertial subrange of turbulence,” NCAR Manuscript 123, Boulder, Colorado, 1966.
³D. K. Lilly, “The representation of small-scale turbulence in numerical

- simulation experiments," in *Proceedings of the IBM Scientific Computing Symposium on Environmental Sciences* (Yorktown Heights, New York, 1967).
- ⁴D. K. Lilly, "The length scale for subgrid-scale parametrization with anisotropic resolution," CTR Annual Research Briefs, pp. 3–9, Center for Turbulence Research, Stanford University/NASA Ames Research Center, 1988.
- ⁵M. Germano, U. Piomelli, P. Moin, and W. H. Cabot, "A dynamic subgrid-scale model," *Phys. Fluids A* **3**, 1760 (1991).
- ⁶U. Piomelli, "Large eddy simulation: present state and future directions," AIAA Technical Report No. 98-0534, 1998.
- ⁷S. Ghosal, T. S. Lund, and P. Moin, "A local dynamic model for large-eddy simulation," CTR Annual Research Briefs, pp. 3–25, Center for Turbulence Research, Stanford University/NASA Ames Research Center, 1992.
- ⁸S. Ghosal, T. S. Lund, P. Moin, and K. Akselvoll, "A dynamic localization model for large-eddy simulation of turbulent flows," *J. Fluid Mech.* **286**, 229 (1995).
- ⁹A. Leonard and G. S. Winckelmans, "A tensor-diffusivity subgrid model for large-eddy simulation," in *Direct and Large-Eddy Simulation III*, edited by P. R. Voke (Kluwer Academic, Dordrecht, 1999), pp. 147–162.
- ¹⁰F. Sarghini, U. Piomelli, and E. Balaras, "Scale-similar models for large-eddy simulations," *Phys. Fluids* **11**, 1569 (1999).
- ¹¹T. J. R. Hughes, L. Mazzei, and K. E. Jansen, "Large eddy simulation and the variational multiscale method," *Comput. Visual Sci. Sci.* **3**, 47 (2000).
- ¹²T. Dubois, F. Jauberteau, and R. Temam, "Solution of the incompressible Navier–Stokes equations by the nonlinear Galerkin method," *J. Sci. Comput.* **8**, 167 (1993).
- ¹³T. Dubois, F. Jauberteau, and R. Temam, "Incremental unknowns, multi-level methods and the numerical simulation of turbulence," *Comput. Methods Appl. Mech. Eng.* **159**, 123 (1998).
- ¹⁴T. Dubois, F. Jauberteau, and R. Temam, *Dynamic Multilevel Methods and the Numerical Simulation of Turbulence* (Cambridge University Press, Cambridge, U.K., 1999).
- ¹⁵T. J. R. Hughes, "Multiscale phenomena: Green's functions, the Dirichlet-to-Neumann formulation, subgrid scale models, bubbles, and the origin of stabilized methods," *Comput. Methods Appl. Mech. Eng.* **127**, 387 (1995).
- ¹⁶T. J. R. Hughes and J. R. Stewart, "A space–time formulation for multi-scale phenomena," *J. Comput. Appl. Math.* **74**, 217 (1996).
- ¹⁷T. J. R. Hughes, G. R. Feijóo, L. Mazzei, and J.-B. Quincy, "The variational multiscale method: A paradigm for computational mechanics," *Comput. Methods Appl. Mech. Eng.* **166**, 3 (1998).
- ¹⁸K. E. Jansen (private communication).
- ¹⁹C. Farhat (private communication).
- ²⁰C. Canuto, M. Y. Hussaini, A. Quarteroni, and T. A. Zang, *Spectral Methods in Fluid Dynamics* (Springer-Verlag, Berlin, 1988).
- ²¹S. A. Orszag and G. S. Patterson, Jr., "Numerical simulation of three-dimensional homogeneous isotropic turbulence," *Phys. Rev. Lett.* **28**, 76 (1972).
- ²²D. K. Lilly, "A proposed modification of the Germano subgrid-scale closure method," *Phys. Fluids A* **4**, 633 (1992).
- ²³N. N. Mansour and A. A. Wray, "Decay of homogeneous isotropic turbulence at low Reynolds number," *Phys. Fluids* **6**, 808 (1994).
- ²⁴A. S. Monin and A. M. Yaglom, *Statistical Fluid Mechanics: Mechanics of Turbulence* (MIT Press, Cambridge, Massachusetts, 1975).